

## Angular-resolved Photoelectron Spectroscopy of Superatom Orbitals of Fullerenes

J. Olof Johansson,<sup>1</sup> Gordon G. Henderson,<sup>1</sup> Françoise Remacle,<sup>2</sup> and Eleanor E. B. Campbell<sup>1,\*</sup>

<sup>1</sup>*EaStCHEM, School of Chemistry, University of Edinburgh, West Mains Road, EH9 3JJ, Scotland*

<sup>2</sup>*Département de Chimie, B6c, Université de Liège, B4000 Liège, Belgium*

(Received 9 September 2011; published 24 April 2012)

Photoelectron angular distributions from both C<sub>60</sub> and C<sub>70</sub> were recorded for low laser intensity femto-second and picosecond pulses. Rich structure is seen for electron kinetic energies that lie below the photon energy. Strong, broad peaks are observed for photoelectron energies corresponding to single-photon ionization of so-called superatom molecular orbitals (SAMOs). The very simple angular distributions measured for these peaks, the close similarity of the spectra observed from C<sub>60</sub> and C<sub>70</sub>, and the comparison with time-dependent density functional theory provide strong support for the SAMO hypothesis.

DOI: 10.1103/PhysRevLett.108.173401

PACS numbers: 36.40.-c, 33.60.+q, 33.80.-b

It is notoriously difficult to obtain information on the excited electronic states of large molecules using conventional multiphoton ionization (MPI) spectroscopy due to the redistribution and rapid equilibration of energy. Fullerenes are a particularly good example of this, showing thermionic electron emission for excitation with ns laser pulses below the ionization potential (IP) [1,2] and even a strong thermal electron emission for excitation with fs pulses [3,4]. Rydberg fingerprint spectroscopy [5] is a technique that avoids the problems associated with conventional MPI. It was first observed in 2001 that fs photoelectron spectra (PES) of small aromatic molecules [6,7] and fullerenes [8] show a rich Rydberg structure that appears largely independent of the laser excitation wavelength. For intense laser excitation, this structure is superimposed on a background of thermal electrons [8,9]. Well-resolved structure can be recorded even for vibrationally hot molecules due to the  $\Delta\nu = 0$  propensity rule (based on Franck–Condon arguments and the structural similarity of the Rydberg states and the cation). Although the mechanisms for populating these Rydberg series are not fully understood, Weber and coworkers have since shown that this technique can be used as a structure-sensitive spectral fingerprint for aromatic molecules [5]. The excited states of fullerenes have recently become of topical interest due to the observation of so-called superatom molecular orbitals (SAMOs) in scanning tunneling spectroscopy (STS) experiments of fullerenes on metal surfaces [10,11]. These are orbitals that have the angular distributions of spherical harmonic functions and are defined by the central potential of the hollow molecular core rather than being defined by the atomic centers. They are thought to be generic for hollow molecules or nanostructures and have important consequences for understanding and tuning the properties of such systems for applications within molecular electronics [11].

In this Letter, we combine Rydberg fingerprint spectroscopy with velocity map imaging (VMI) to obtain angular-resolved PES from neutral fullerenes. The results

provide strong evidence for the excitation of the *s*-SAMO and provide a stringent test of the theoretical models being developed to study the electronic properties of these interesting nanosystems [11,12].

An effusive molecular beam of purified C<sub>60</sub> or C<sub>70</sub> is produced in a resistively-heated oven at a temperature of 500 °C and introduced to the laser-interaction region of a combined linear time-of-flight mass spectrometer/VMI photoelectron spectrometer (arranged at 180°), similar to the setup described in [4]. A Ti:sapphire regenerative amplifier producing 800 nm pulses with a duration of 120 fs (9 nm bandwidth) and 1 kHz repetition rate with maximum output energy of 3.8 mJ is used. The fundamental output from the laser was frequency doubled in a beta-barium borate (BBO) crystal yielding 120 fs, 400 nm light (3 nm bandwidth). Bandwidth-limited 4 ps pulses of 401 nm wavelength (5 cm<sup>-1</sup> bandwidth) were produced with a second harmonic bandwidth converter and tunable fs pulses (500–1000 nm) with a Topas-white noncollinear optical parametric amplifier. The raw VMI images were inverted using pBASEX [13] and checked for consistency with BASEX [14] and POP [15] (modified to include up to the tenth Legendre polynomial in the inversion procedure).

For the calculations, C<sub>60</sub> was optimized without imposing symmetry at the B3LYP/6-31+G(d) and B3LYP/6-311+G(d) levels [16]. The equilibrium geometry was computed to belong to the point group *I<sub>h</sub>*. In order to study the excited states of C<sub>60</sub>, time-dependent density functional theory (TD-DFT) computations were undertaken for the two basis sets for a band of 200 excited states above the ground state, with and without imposing *I<sub>h</sub>* symmetry. The four levels of computation gave the same excitation energies within numerical precision. To examine even higher-lying states, a TD-DFT computation for a band of 500 excited states was carried out at the B3LYP/6-31+G(d) level with the *I<sub>h</sub>* symmetry imposed. The first *s*-like excited state falls within the band of 200 excited states, but the higher excited states do not. The excitation energies to the first *s*-like state computed for the band of

200 excited states and for the band of 500 excited states are identical.

Inverted VMI images from  $C_{60}$  after 120 fs, 400 nm and 120 fs, 800 nm laser excitation are shown in Fig. 1. The laser intensities were low enough for each wavelength to only observe singly charged parent ions in the mass spectra [see inset in Fig. 2(a)]. Even for the low laser intensities used to obtain the data in Fig. 1, the signal consists of two components: a peak structure superimposed on a thermal background. The thermal background has been discussed in detail previously [4]. Here we focus on the resolved peak structure, which dominates at low laser intensities. In order to separate the two components, the VMI image is divided into angular segments of  $10^\circ$  intervals and the thermal background is subtracted leaving PES such as those illustrated in Fig. 2 for the  $0\text{--}10^\circ$  angular interval obtained from  $C_{60}$  and  $C_{70}$  for different wavelengths and pulse durations. For comparison, the spectrum of excited states obtained from the TD-DFT calculations is also shown in Fig. 2(b). The energy scale was converted to match the PES by subtracting the computed binding energy from the photon energy corresponding to 400 nm.

The spectra in this angular interval are in agreement with the time-of-flight photoelectron spectra reported previously by Boyle *et al.* [8,17]. It was shown earlier that the structure can be identified with single-photon ionization of Rydberg states [17], as is the case for Rydberg fingerprint spectroscopy [5]. Here we focus on the intense broad peaks that are clearly visible in the 400 nm spectra (identified as peaks I–IV in Fig. 2). The binding energies of the peaks are listed in Table I. Peaks corresponding to states with the same binding energies are found for excitation with 400 to 600 nm and peaks II–IV are found in the spectra taken with 700 to 800 nm where the photon energy is too low to single-photon ionize from the state corresponding to peak I. Although the higher energy peaks (III and IV) are better resolved in the  $C_{60}$  ps spectrum compared to the fs data, the full width at half maximum (FWHM) of peaks I and II does not change significantly.

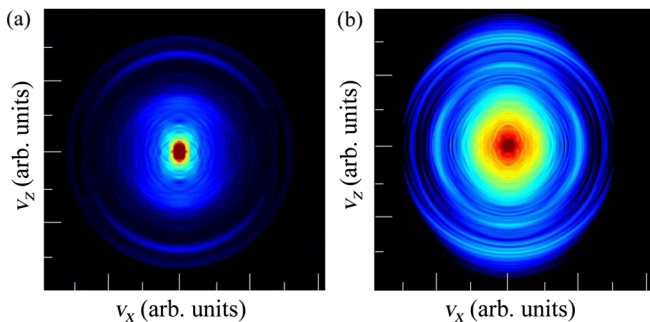


FIG. 1 (color online). Inverted VMI images for  $C_{60}$  after (a) 120 fs, 400 nm laser excitation ( $3 \times 10^{11}$  W/cm $^2$ ) and (b) 120 fs, 800 nm ( $3.7 \times 10^{12}$  W/cm $^2$ ). The laser polarization direction was parallel to the  $z$ -axis.

The Rydberg structure in  $C_{60}$  PES was earlier assigned to Rydberg series with  $\ell = 3, 5,$  and  $7$  [8] based on the agreement of electron binding energies with values estimated from solving the Schrödinger equation using a simple jellium potential. Peak I did not fit the main series and was tentatively assigned to the  $4p$  Rydberg state (where the number 4 indicates the number of radial nodes + 1). Peaks II, III, and IV were assigned to the  $4d, 3h,$  and  $4g$  states. The PADs, reported here, in combination with the recent STS observations of SAMOs [10] and more recent DFT [11] and Hartree-Fock [12] calculations, as well as the TD-DFT calculations presented here, lead us to revise these assignments. One can consider the SAMO states to be

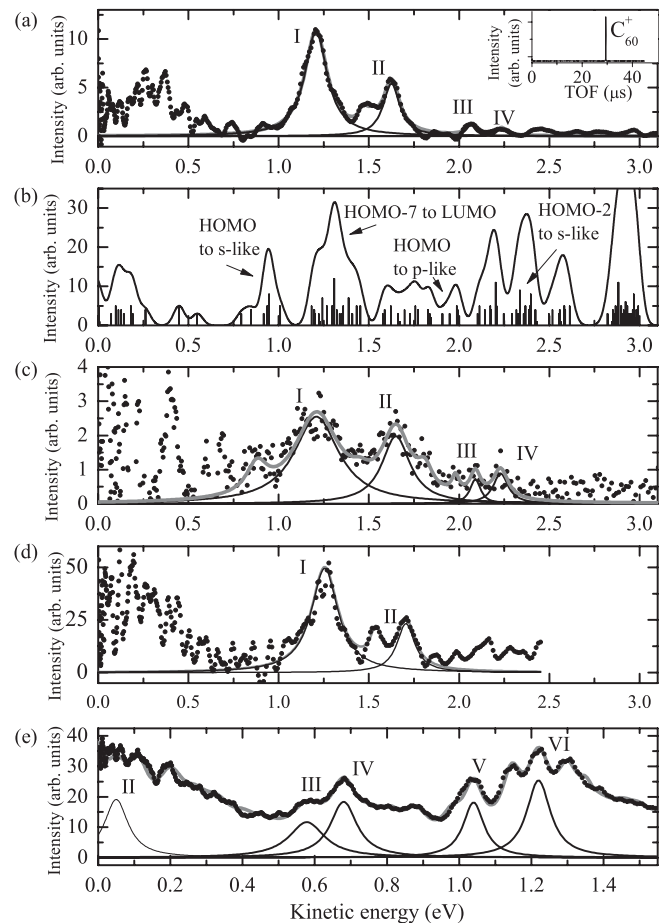


FIG. 2. Angle-resolved PES for polar angle interval  $0\text{--}10^\circ$  obtained by exciting (a)  $C_{60}$  with 400 nm, 120 fs laser pulses of intensity  $3 \times 10^{11}$  W/cm $^2$ . (b) Calculated spectrum of excited states of  $C_{60}$  from TD-DFT calculations. The solid line was obtained by convoluting each state with a Gaussian function. The energy scale has been converted to photoelectron kinetic energy to compare to experimental PES obtained for 400 nm light. (c) Same as (a) but using 401 nm, 4 ps ( $5\text{ cm}^{-1}$  bandwidth) laser light of intensity  $7 \times 10^{10}$  W/cm $^2$ ; (d)  $C_{70}$  400 nm, 120 fs and (e)  $C_{60}$  800 nm, 120 fs and intensity  $3.7 \times 10^{12}$  W/cm $^2$ . The inset in (a) shows a time-of-flight mass spectrum obtained for the same laser conditions as in (a).

TABLE I. Average value of peak binding energies obtained for all wavelengths. Values for  $C_{70}$  are given in parentheses.

Peak	Binding energy (eV)
I	$1.90 \pm 0.01$ ( $1.86 \pm 0.02$ )
II	$1.47 \pm 0.02$ ( $1.41 \pm 0.02$ )
III	$1.02 \pm 0.01$
IV	$0.87 \pm 0.02$

precursors to the Rydberg series. However, in contrast to the Rydberg states, the electron density of the SAMOs resides substantially inside the hollow fullerene cage [10]. The spatial angular distributions of SAMOs follow spherical harmonics because the electron moves in the central field of its image charge, which arises due to short-range exchange and correlation effects caused by the close proximity to the other valence electrons and is a consequence of the hollow geometry [10]. In contrast, in a molecular Rydberg state, the electron is sufficiently far away from the other electrons and therefore only experiences the long-range Coulomb potential, creating the central potential required for maintaining  $\ell$  as a good quantum number.

The integrated peak intensities for peaks I–VI presented in Fig. 2 are plotted as a function of polar angle in Fig. 3. For a single pulse of linearly polarized light, single-photon ionization of a randomly oriented target results in a photoelectron angular distribution (PAD),  $I(\theta)$ , for a specific kinetic energy according to [18]

$$I(\theta) = \frac{\sigma_{\text{total}}}{4\pi} [1 + \beta P_2(\cos\theta)], \quad (1)$$

where  $\sigma_{\text{total}}$  is the angle-integrated cross section,  $\beta$  is the anisotropy parameter (which takes on values between  $-1$  and  $2$ ), and  $P_2$  is the second order Legendre polynomial. In the atomic case, where the orbital angular momentum quantum number  $\ell$  is a good quantum number,  $\beta$  can be determined by the Cooper-Zare formula [19]. If the initial state is an  $s$ -state, implying that the angular momentum of the outgoing electron can only take on the value of  $\ell = 1$ ,  $\beta$  should equal two (in the absence of significant electron correlation effects). For higher angular momentum states, there will be interference between the outgoing channels leading to a value of  $\beta$  that varies with the kinetic energy of the outgoing electron.

The PADs shown in Fig. 3 can all be fitted with Eq. (1), confirming that the structure in the PES is produced from single-photon ionization from a wide range of electronically excited states. The extracted values of  $\beta$  are plotted as a function of electron kinetic energy in Fig. 4. It was not possible to reproduce the measured PADs for these peaks using the original assignment [8] and calculations based on the simple jellium potential. The most intense broad peak seen in the spectra, peak I (Fig. 2), and the smaller peak IV have values of beta that are very close to 2.0 and do not show a strong variation with electron kinetic energy. It therefore seems reasonable to assign those peaks to  $s$ -states. Further support for the assignment is given by the TD-DFT calculations which show an excited state comprised entirely of the  $s$ -SAMO with a binding energy of 2.15 eV, in reasonable agreement with the experimental value of  $1.90 \pm 0.01$  eV for peak I. The calculations also show a higher-lying  $s$ -SAMO state with a binding energy of 0.78 eV, which is in reasonable agreement with the binding energy of peak IV ( $0.87 \pm 0.02$  eV).

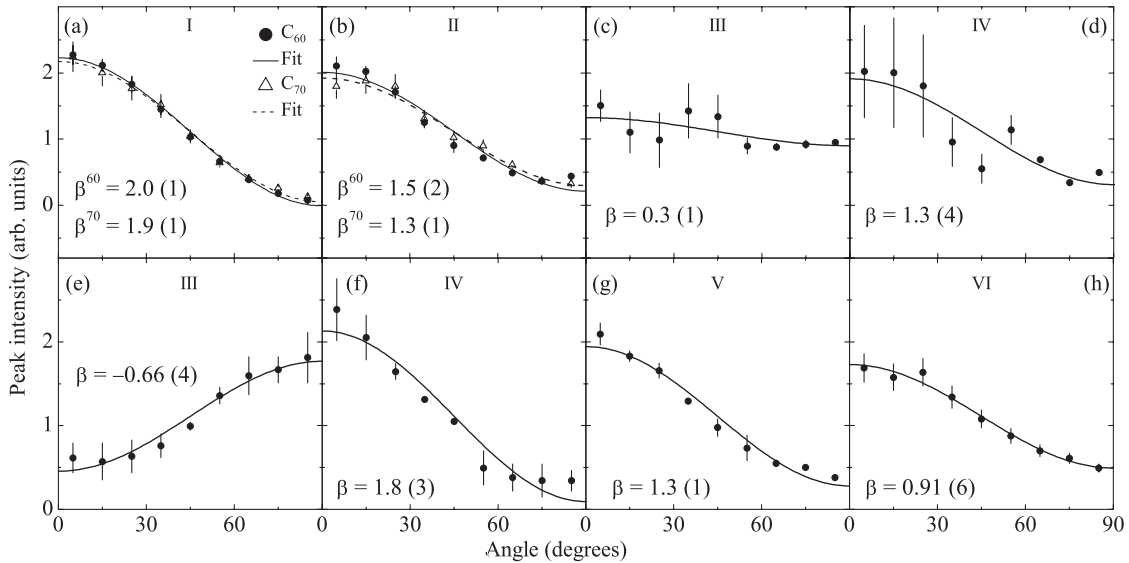


FIG. 3. PADs corresponding to the marked peaks in Fig. 2 obtained by exciting with (a)–(d) 400 nm, 120 fs laser pulses of intensity  $3 \times 10^{11}$  W/cm<sup>2</sup> and (e)–(h) 800 nm, 120 fs and intensity  $3.7 \times 10^{12}$  W/cm<sup>2</sup>. The angular dependence was fitted using Eq. (1) to determine  $\beta$ .

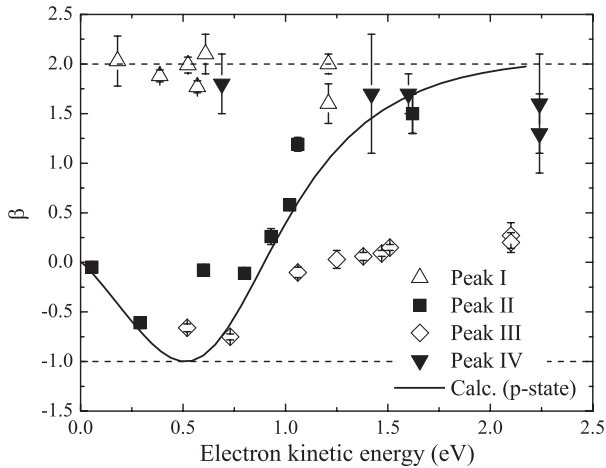


FIG. 4. Anisotropy parameter,  $\beta$ , as a function of photoelectron kinetic energy. The dashed lines show the minimum and maximum possible value of  $\beta$  for a single-photon ionization process. Peaks I and IV are identified as arising from  $s$ -SAMO states based on their binding energies and  $\beta \approx 2$ . The solid line shows the calculated  $\beta$  values obtained for the  $p$ -state using Eq. (2).

The PADs for peaks II and III do vary with kinetic energy and can be assigned to higher angular momentum states. The calculations show a broad band of states above the  $s$ -state and it is not clear which states the observed peaks correspond to. Based on the energy difference between peak I and II, the HOMO-7 to LUMO excited state with binding energy 1.79 eV could be assigned to peak II ( $1.47 \pm 0.02$ ). On the other hand, it is also possible that a pure  $p$ -state with binding energy 1.26 eV, identified in the calculations, could give rise to peak II. We have used a simple model to calculate the angular distributions of the emitted electrons using plane waves as the final wave functions for the outgoing electrons. The distribution of emitted photoelectrons as a function of momentum  $\mathbf{k}$ , in spherical coordinates, can be described as

$$I(k, \theta, \phi) \propto \left| \int \psi_i^* \hat{\mu} e^{-2\pi i \mathbf{k} \cdot \mathbf{r}} d\mathbf{r} \right|^2, \quad (2)$$

where  $\hat{\mu}$  is the dipole operator and  $\psi_i$  is the orbital of the ionized electron computed at the TD-DFT level. When the calculated PAD for the  $p$ -state is compared to the experimental data in Fig. 4, there is a striking agreement with the PAD for peak II. It is therefore tempting to assign peak II as a  $p$ -SAMO state, although further calculations are needed for an accurate assignment.

It is striking that there are two prominent peaks in the  $C_{70}$  PES that are very close in energy to peaks I and II in the  $C_{60}$  spectra and that show almost identical PADs (the signal to noise ratio is too poor to reliably extract information from higher energy peaks). The DFT calculations presented in Ref. [11] also predict the  $3s$  SAMO state of  $C_{70}$  to have a lower binding energy than that of  $C_{60}$ , by

ca. 0.1 eV [11]. The experimental results are in reasonable agreement with this, lying ca. 0.04 eV and 0.06 eV lower in energy for peak I and II, respectively. TD-DFT calculations for  $C_{70}$  are underway.

In conclusion, we have presented angle-resolved PES of gas-phase  $C_{60}$  and  $C_{70}$  after fs and ps laser excitation. Some of the most prominent observed peaks in the PES were interpreted as single-photon ionization of SAMOs, diffuse molecular orbitals predicted to be centered on the core of hollow molecules [11]. This assignment was based on the comparison of relative binding energies with theoretical calculations and, in particular, the PADs that allowed us to clearly identify two  $s$ -SAMO states. The assignment of peaks II and III is less certain but the kinetic energy dependence of the anisotropy parameter,  $\beta$ , provides a stringent test of theoretical calculations. The comparison with TD-DFT calculations indicates that peak II could be a  $p$ -SAMO state. The powerful combination of fs Rydberg fingerprint spectroscopy and photoelectron VMI that we demonstrate here can provide detailed information about excited electronic states of complex molecules in the gas phase that cannot be obtained readily with other methods. The fullerene results that are presented will hopefully stimulate theoretical efforts to obtain a greater understanding of the properties of these novel electronic states which, in turn, could stimulate the development of new materials for applications in molecular electronics.

The authors thank A. V. Gromov for supplying the purified  $C_{70}$  sample, A. Molberg and X. Guo for help with some of the measurements, T. Ridley, K.P. Lawley, H. Petek, J. Berakdar, and Y. Pavlyukh for helpful discussions. Financial support from EaStCHEM is gratefully acknowledged. F. R. is a Director of Research of Fonds National de la Recherche Scientifique, Belgium.

\*eleanor.campbell@ed.ac.uk

- [1] E. E. B. Campbell, G. Ulmer, and I. V. Hertel, *Phys. Rev. Lett.* **67**, 1986 (1991).
- [2] F. Lepine, B. Climen, M. Lebeault, and C. Bordas, *Eur. Phys. J. D* **55**, 627 (2009).
- [3] K. Hansen, K. Hoffmann, and E. Campbell, *J. Chem. Phys.* **119**, 2513 (2003).
- [4] M. Kjellberg, O. Johansson, F. Jonsson, A. V. Bulgakov, C. Bordas, E. E. B. Campbell, and K. Hansen, *Phys. Rev. A* **81**, 023202 (2010).
- [5] J. Gosselin and P. Weber, *J. Phys. Chem. A* **109**, 4899 (2005).
- [6] M. Tsubouchi, B. J. Whitaker, L. Wang, H. Kohguchi, and T. Suzuki, *Phys. Rev. Lett.* **86**, 4500 (2001).
- [7] C. Schick and P. Weber, *J. Phys. Chem. A* **105**, 3735 (2001).
- [8] M. Boyle, K. Hoffmann, C. P. Schulz, I. V. Hertel, R. D. Levine, and E. E. B. Campbell, *Phys. Rev. Lett.* **87**, 273401 (2001).

- [9] M. Kjellberg, A. V. Bulgakov, M. Goto, O. Johansson, and K. Hansen, *J. Chem. Phys.* **133**, 074308 (2010).
- [10] M. Feng, J. Zhao, and H. Petek, *Science* **320**, 359 (2008).
- [11] J. Zhao, M. Feng, J. Yang, and H. Petek, *ACS Nano* **3**, 853 (2009).
- [12] Y. Pavlyukh and J. Berakdar, *Chem. Phys. Lett.* **468**, 313 (2009).
- [13] G. A. Garcia, L Nahon, and I. Powis, *Rev. Sci. Instrum.* **75**, 4989 (2004).
- [14] V. Dribinski, A. Ossadtchi, V. Mandelshtam, and H. Reisler, *Rev. Sci. Instrum.* **73**, 2634 (2002).
- [15] G. M. Roberts, J. L. Nixon, J. Lecointre, E. Wrede, and J. R. R. Verlet, *Rev. Sci. Instrum.* **80**, 053104 (2009).
- [16] M. J. Frisch, G. W. Trucks, H. B. Schlegel, G. E. Scuseria, M. A. Robb, J. R. Cheeseman, G. Scalmani, V. Barone, B. Mennucci, G. A. Petersson, H. Nakatsuji, M. Caricato, X. Li, H. P. H., A. F. Izmaylov, J. Bloino, G. Zheng, J. L. Sonnenberg, M. Hada, M. Ehara, K. Toyota, R. Fukuda, J. Hasegawa, M. Ishida, T. Nakajima, Y. Honda, O. Kitao, H. Nakai, T. Vreven, J. A. Montgomery, J. E. P, Jr., F. Ogliaro, M. Bearpark, J. J. Heyd, E. Brothers, K. N. Kudin, V. N. Staroverov, R. Kobayashi, J. Normand, K. Raghavachari, A. Rendell, J. C. Burant, S. S. Iyengar, J. Tomasi, M. Cossi, N. Rega, J. M. Millam, M. Klene, J. E. Knox, J. B. Cross, V. Bakken, C. Adamo, J. Jaramillo, R. Gomperts, R. E. Stratmann, O. Yazyev, A. J. Austin, R. Cammi, C. Pomelli, J. W. Ochterski, R. L. Martin, K. Morokuma, V. G. Zakrzewski, G. A. Voth, P. Salvador, J. J. Dannenberg, S. Dapprich, A. D. Daniels, J. Farkas, B. Foresman, J. V. Ortiz, J. Cioslowski, D. J. Fox, Gaussian 09 Revision A.1. 2009
- [17] M. Boyle, T. Laarmann, K. Hoffmann, M. Heden, E. Campbell, C. Schulz, and I. Hertel, *Eur. Phys. J. D* **36**, 339 (2005).
- [18] K. Reid, *Annu. Rev. Phys. Chem.* **54**, 397 (2003).
- [19] J. Cooper and R. Zare, *J. Chem. Phys.* **48**, 942 (1968).